Air Force Institute of Technology

AFIT Scholar

11-25-2019

Effect of Ar(3p^{5}4p; 2p)+M -> Ar(3p^{5}4s; 1s)+M branching ratio on optically pumped rare gas laser performance

Daniel J. Emmons II
Air Force Institute of Technology

David E. Weeks
Air Force Institute of Technology

Recommended Citation

Effect of Ar(3p⁵4p; 2p)+M → Ar(3p⁵4s; 1s)+M branching ratio on optically pumped rare gas laser performance

D. J. EMMONS* [iD] AND D. E. WEEKS

Dept. of Physics, Air Force Institute of Technology, 2950 Hobson Way, Wright-Patterson AFB, OH 45433, USA

*daniel.emmons@afit.edu

Abstract: Optically pumped rare gas laser performance is analyzed as a function of the $Ar(3p^54p; 2p) + M \rightarrow Ar(3p^54s; 1s) + M$ branching ratios. Due to the uncertainty in the branching ratios, a sensitivity study is performed to determine the effect on output and absorbed pump laser intensities. The analysis is performed using a radio frequency dielectric barrier discharge as the source of metastable production for a variety of Argon in Helium mixtures over pressures ranging from 200 to 500 Torr. Peak output laser intensities show a factor of 7 increase as the branching ratio is increased from 0.25 to 1.00. The collection of Ar^* in $Ar(1s_4)$ is inversely proportional to the branching ratio and decreases output laser intensity by reducing the density of species directly involved with lasing.

1. Introduction

An optically pumped rare gas laser (OPRGL) with Ar as the rare gas uses a diode laser to pump metastable $Ar(1s_5)$ atoms to the $Ar(2p_9)$ energy level [1]. Near-atmospheric pressures are required for rapid collisional relaxation from $Ar(2p_9)$ to $Ar(2p_{10})$ to create a population inversion and subsequent lasing between $Ar(2p_{10})$ and $Ar(1s_5)$, as displayed in Fig. 1. Additionally, the broad linewidths of diode pump lasers call for high pressures to broaden the relatively narrow absorption linewidth. Optical gain depends on the diode laser absorption, which depends on the $Ar(1s_5)$ density [2,3]. A gas discharge is used to produce sufficient metastable densities, which act as the ground state of the OPRGL system.

Several kinetic studies of OPRGLs have been performed recently [2–5]. One study found that at atmospheric pressures, a mixture of approximately 1% Ar in He provides the largest efficiency, defined as the output power divided by sum of pump and discharge power [3]. A separate kinetic analysis determined the effect of metastable density on output laser powers, predicting output intensities above 1 kW/cm² for metastable densities on the order of 10^{13} cm^{-3} and pump laser intensities above 2 kW/cm² [4].

An experimental and computational analysis of an OPRGL using microwave resonator-driven microplasmas as the metastable source measured a laser output of 22 mW for an absorbed pump power of 40 mW and an estimated metastable density of 3×10^{12} cm^{-3} [2]. This measurement provides an optical efficiency of approximately 55%. The gain, G, was found to be linear with respect to metastable density, following $[Ar(1s_5)]/G = 4 \times 10^{12}$ cm^{-2}, measured at 760 Torr for a mixture of 2% Ar in He. Additionally, a computational analysis of the laser kinetics found a better fit to the data when an Arrhenius temperature scaling was applied to the neutral collision transfer rates between the different excited Ar species [2].

While the rate coefficients for collisional de-excitation following $Ar(2p) + M \rightarrow Ar(1s) + M$ are well documented [6,7], the branching ratios to the specific $Ar(1s)$ levels ($1s_5$-$1s_2$) are uncertain. Additionally, as discussed in [6], the rate coefficients depend strongly on diabatic coupling near crossings of the potential energy curves, not just the energy difference between states. Due to the uncertainty in the branching ratios, previous kinetic studies of optically pumped rare gas laser performance have assumed that all $Ar(2p) + M \rightarrow Ar(1s) + M$ collisions channel directly
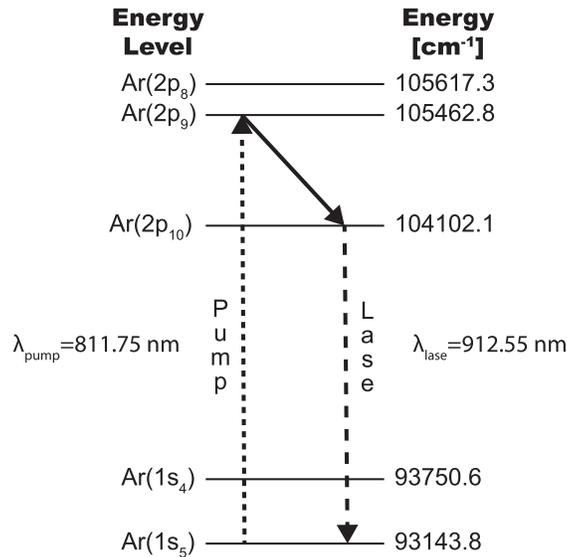
Fig. 1. A diagram of the Ar energy levels pertinent to an optically pumped rare-gas laser. A diode laser optically pumps metastable $Ar(1s_5)$ to $Ar(2p_9)$, followed by collisional relaxation to $Ar(2p_{10})$ and subsequent lasing to $Ar(1s_5)$. The $Ar(1s_4)$ and $Ar(2p_8)$ levels are important to OPRGL kinetics due to their proximity to $Ar(1s_5)$ and $Ar(2p_9)$, respectively.

to $Ar(1s_5)$ bypassing the other $Ar(1s)$ levels [2–5]. In this paper we analyze the effect of the $Ar(2p) + M \rightarrow Ar(1s) + M$ branching ratios on OPRGL performance with a radio frequency dielectric barrier discharge (RF-DBD) as the source of metastable production.

This OPRGL analysis is based on metastable densities simulated for the RF-DBD outlined in [8] and [9] with a peak applied voltage of 500 V and a driving frequency of 13.56 MHz. A lower voltage was selected to ensure an α-mode discharge over all pressures and mixtures, which corresponds to metastable densities on the order of 10^{11} cm^{-3}. The relatively low metastable densities for this RF-DBD are considerably suboptimal for laser performance, but instead allow for a study of laser intensity trends as a function of pressure, Ar-He mixture, and branching ratio. Alternative discharges are capable of yielding elevated metastable densities necessary for high power OPRGL laser performance, as recently demonstrated by the 4 W continuous-wave OPRGL produced using a nanosecond pulsed discharge with time averaged $Ar(1s_5)$ densities above 10^{13} cm^{-3} [10,11]. Additionally, metastable densities on the order of 10^{12} cm^{-3} have recently been observed in a 20 kHz DBD [12].

2. Model

Gas discharge simulations are performed using the zero-dimensional plasma kinetics model, ZDPlasKin [13], which employs BOLSIG+ for electron energy distribution function calculations [14]. The zero-dimensional kinetic model for a RF-DBD is outlined in [9], and the reaction rate package is outlined in [15]. The reaction rate package includes electron impact, recombination, two-heavy-body, three-heavy-body, and radiative rate coefficients. Species relevant to a five-level laser model are analyzed: $Ar(1s_5)$, $Ar(1s_4)$, $Ar(2p_{10})$, $Ar(2p_9)$, and $Ar(2p_8)$. To limit the rate package complexity, the remaining $Ar(1s)$ and $Ar(2p)$ levels are not included in the kinetics model. A neutral gas temperature of 440 K is used for all mixtures and pressures based on measurements of a similar RF-DBD [16]. This gas temperature corresponds to a rate coefficient

of 3.7×10^{-13} cm^3/s for the $Ar(1s_4) + He \rightarrow Ar(1s_5) + He$ reaction, extrapolated from the temperature dependence of the rate provided by [7].

In addition to the reactions provided in [15], transfer rates due to pump laser absorption and circulating laser intensity are included [4,17–19]. The absorbed pump intensity, I_a, and corresponding reaction rate from $Ar(1s_5)$ to $Ar(2p_9)$, W_a, follow

$$I_a = I_p \int d\nu \, g_p(\nu) \left\{ 1 - \exp\left[-\left([Ar(1s_5)] - \frac{5}{7}[Ar(2p_9)] \right) \sigma_{pl}(\nu) \ell_g \right] \right\}$$
$$\left\{ 1 + R_p \exp\left[-\left([Ar(1s_5)] - \frac{5}{7}[Ar(2p_9)] \right) \sigma_{pl}(\nu) \ell_g \right] \right\}, \tag{1}$$

$$W_a = \frac{I_a}{E_{pl}\ell_g}, \tag{2}$$

where $I_p = 1$ kW/cm^2 is the incident pump laser intensity, $[Ar^*]$ is the Ar^* density, $\ell_g = 5.1$ cm is the length of gain medium, R_p is the pump laser reflectivity (assumed to be 1), and E_{pl} is the pump transition energy [4,17,19]. In this analysis, the pump delivery and mode overlap factors are ignored (assumed to be 1). The line shape of the pump laser, $g_p(\nu)$, is assumed to be a Gaussian distribution with a FWHM linewidth of 30 GHz [19]. The absorption cross section, $\sigma_{pl}(\nu)$, is assumed to have a Lorentzian line shape with a pressure broadening coefficient of $17\sqrt{T_{gas}/300}$ MHz/Torr, where T_{gas} is the neutral gas temperature in Kelvin [2]. This pressure broadening coefficient is assumed to be independent of Ar/He mixture. At 760 Torr and 300 K, the peak absorption cross section is calculated to be $\sigma_{pl} \approx 4.3 \times 10^{-13}$ cm^2, which is close to the value of 4.5×10^{-13} cm^2 provided by [3].

The average two-way circulating laser intensity, I_l, and corresponding reaction rate from $Ar(2p_{10})$ to $Ar(1s_5)$, W_l, follow

$$\frac{dI_l}{dt} = \frac{I_l c}{2\ell_c} \left\{ R_l R_{oc} T_r^2 \exp\left[2\left([Ar(2p_{10})] - \frac{3}{5}[Ar(1s_5)] \right) \sigma_{ul} \ell_g \right] - 1 \right\}, \tag{3}$$

$$W_l = \sigma_{ul} \left([Ar(2p_{10})] - \frac{3}{5}[Ar(1s_5)] \right) \frac{I_l}{E_{ul}}, \tag{4}$$

where R_l is back mirror reflectivity (assumed to be 1), $R_{oc} = 0.95$ is the output coupler reflectivity, T_r is the one-way cavity transmission (assumed to be 1), ℓ_c is the cavity length (assumed to be equal to ℓ_g), and E_{ul} is the output laser transition energy [4,17]. A threshold gain of approximately 0.02 cm^{-1} is calculated for this system. The gain cross section is calculated by $\sigma_{ul} = 5.0 \times 10^{-13} (N_{atm}/N)$ cm^2, where N_{atm} is the number density at 760 Torr and 300 K and N is the number density used in the simulations [3]. The output laser intensity, I_o, follows [18]

$$I_o = \frac{W_l E_{ul} \ell_g (1 - R_{oc}) T_r \exp\left[\left([Ar(2p_{10})] - \frac{3}{5}[Ar(1s_5)] \right) \sigma_{ul} \ell_g \right]}{\left\{ \exp\left[\left([Ar(2p_{10})] - \frac{3}{5}[Ar(1s_5)] \right) \sigma_{ul} \ell_g \right] - 1 \right\} \left\{ 1 + T_r^2 R_{oc} \exp\left[\left([Ar(2p_{10})] - \frac{3}{5}[Ar(1s_5)] \right) \sigma_{ul} \ell_g \right] \right\}}. \tag{5}$$

For this study, the branching ratio is defined as the ratio of the rate coefficient for $Ar(2p) + M \rightarrow Ar(1s_5) + M$ relative to the total rate coefficient for $Ar(2p) + M \rightarrow Ar(1s) + M$ excluding quenching to the ground state. All $Ar(2p)$ species are assumed to have the same branching ratio to simplify the analysis. Since $Ar(1s_4)$ is the only other $Ar(1s)$ level modeled in this analysis, the branching

ratio can be described by

$$\text{branching ratio} = \frac{k_{Ar(2p)+M \to Ar(1s_5)+M}}{k_{Ar(2p)+M \to Ar(1s_5)+M} + k_{Ar(2p)+M \to Ar(1s_4)+M}}. \tag{6}$$

To limit complexity, the $Ar(1s_3)$ and $Ar(1s_2)$ levels are not included in the kinetics model, but their inclusion would provide additional kinetic pathways from $Ar(2p)$ to $Ar(1s)$ that should be incorporated in future efforts. The discharge simulations outlined in [15] and [9] assumed a branching ratio of 0.50. However, previous OPRGL simulations have assumed a branching ratio of 1.00 [2–5]. These previous simulations with different branching ratios used various types of discharges and conditions, which makes a comparison of the results difficult. This study uses a single gas discharge to analyze the effect of the branching ratio on discharge and laser kinetics for varying mixtures and pressures.

Before the inclusion of the laser rates due to the introduction of the pump laser, zero-dimensional simulations of the RF-DBD are carried out to an initial steady-state, providing the densities $[Ar^*]_d$ and discharge conditions defined as *discharge*. Then, the laser rates are included and the simulations are executed to a new steady-state where the densities and laser intensities are constant in time, providing the densities $[Ar^*]_l$ and discharge conditions defined as *laser*.

3. Results

Gas discharge simulations are performed for an RF-DBD with an applied voltage of 500 V peak for a variety of Ar in He mixtures and pressures ranging from 200-500 Torr before inclusion of the laser rates. The discharge metastable densities in the bulk plasma show a peak of approximately 7.0×10^{11} cm^{-3} near 15% Ar in He at 200 Torr, as displayed in Fig. 2 for a branching ratio of 0.50. The metastable density is reduced as the pressure is increased and the peak metastable density shifts to a lower Ar-fraction, following the trend in the steady-state reduced electric field, E/N [8,9]. At 500 Torr, the peak metastable density is reduced to $\sim 2.4 \times 10^{11}$ cm^{-3}, occurring at an Ar-fraction of approximately 10%. This decrease in metastable density with increasing pressure is due to elevated metastable loss rates, primarily through excimer formation via $Ar(1s_5) + Ar + M \to Ar_2^* + M$. For the discharge scenario modeled, the peak metastable densities for all pressures in the range of 200-500 Torr are on the order of 10^{11} cm^{-3}. A slight variation in discharge metastable density is observed with respect to the branching ratio, with an average relative difference under 5% for all mixtures and pressures when compared to the branching ratio of 0.50. Discharge metastable densities are not strongly dependent on the branching ratio due to the relatively low metastable production rates from collision relaxation of $Ar(2p)$.

After laser initiation, a large boost in $Ar(2p)$ densities is observed as a result of pump laser absorption. This increase in $Ar(2p)$ densities elevates the $Ar(2p) + M \to Ar(1s) + M$ rates, forcing the laser kinetics to be strongly dependent on the branching ratio. For example, the $Ar(2p_9) + M \to Ar(1s_4) + M$ loss rate relative to the $Ar(2p_9) + M \to Ar(2p_{10}) + M$ laser rate for the 460 Torr, 8% Ar-fraction scenario declines from 0.3 to 0.0 as the branching ratio rises from 0.0 to 1.0. As displayed in Fig. 3, the absorbed pump laser intensity is proportional to the branching ratio. As the branching ratio increases, the excited Ar species densities collected in $Ar(1s_4)$ are reduced. The peak absorption over all pressures and mixtures is raised from approximately 4.7 to 31.2 W/cm^2 as the branching ratio increases from 0.25 to 1.00. Additionally, the pressure corresponding to peak absorption shifts from 400 to 440 Torr as the branching ratio increases.

The output laser intensity, as displayed in Fig. 4, also shows an increase with increasing branching ratio. Similar to the pump laser absorption, the peak laser output occurs at a higher pressure for larger branching ratios (Table 1). As the pressure increases, the $Ar(2p) + M \to Ar(1s) + M$ rates also increase. For lower branching ratios, this rate increase is detrimental
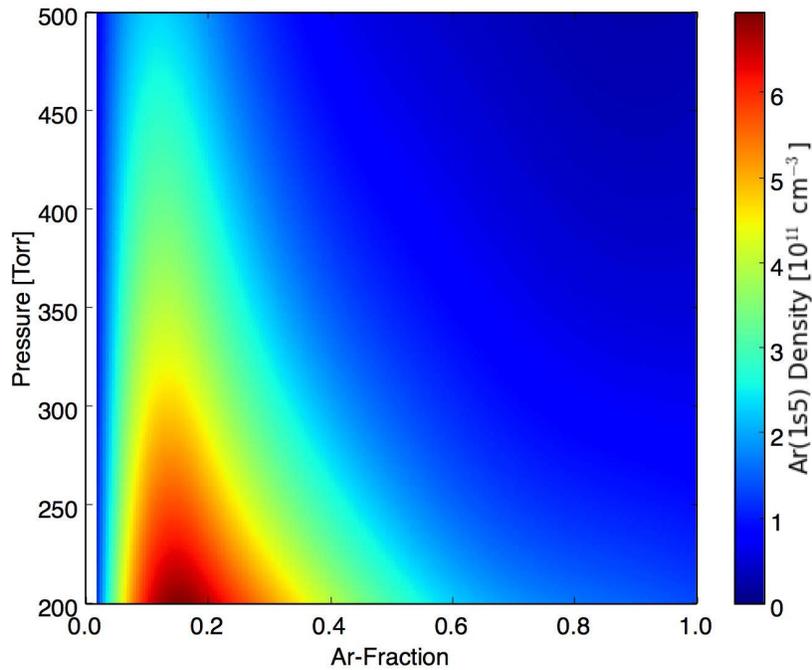
Fig. 2. Simulated metastable densities as a function of Ar-fraction and pressure for a branching ratio of 0.50 [9]. Initial metastable densities calculated using branching ratios of 0.25, 0.75, and 1.00 resulted in average relative differences under 5%.

to laser performance because of a loss in excited species densities directly involved with laser performance: $Ar(1s_5)$, $Ar(2p_9)$, and $Ar(2p_{10})$. This loss is caused by quenching from $Ar(2p)$ to $Ar(1s_4)$ and subsequent pooling at $Ar(1s_4)$. As the branching ratio increases, the rate to $Ar(1s_4)$ decreases while the rate to $Ar(1s_5)$ increases, thereby decreasing the detrimental effect of the pressure increase. Additionally, the $Ar(2p_9) + M \rightarrow Ar(2p_{10}) + M$ collisional relaxation rate and pump laser absorption linewidth both increase with increasing pressure, enhancing laser performance. No lasing occurs for Ar rich mixtures with reduced metastable densities at the lower branching ratios.

Table 1. Parameters associated with peak output laser intensities as a function of branching ratio.

Branching Ratio	Peak Laser Intensity [W/cm²]	Pressure [Torr]	Ar-Fraction	Absorbed Pump Intensity [W/cm²]	Optical to Optical Conversion Efficiency
0.25	2.1	440	0.08	4.7	0.46
0.50	3.1	460	0.08	6.5	0.47
0.75	5.1	480	0.08	10.5	0.48
1.00	14.2	500	0.12	30.8	0.46

A peak output intensity of approximately 2.1 W/cm² is observed at 440 Torr for a branching ratio of 0.25, while a peak of 14.2 W/cm² is predicted at 500 Torr for a branching ratio of 1.00 (Table 1). The peaks occur at an Ar-fraction of 12% for the 1.00 branching ratio and at 8% Ar-fraction for the other branching ratios. This nearly 7 fold increase in peak laser intensity highlights the importance of the branching ratio in OPRGL operation.

(a) Branching ratio = 0.25

(b) Branching ratio = 0.50

(c) Branching ratio = 0.75
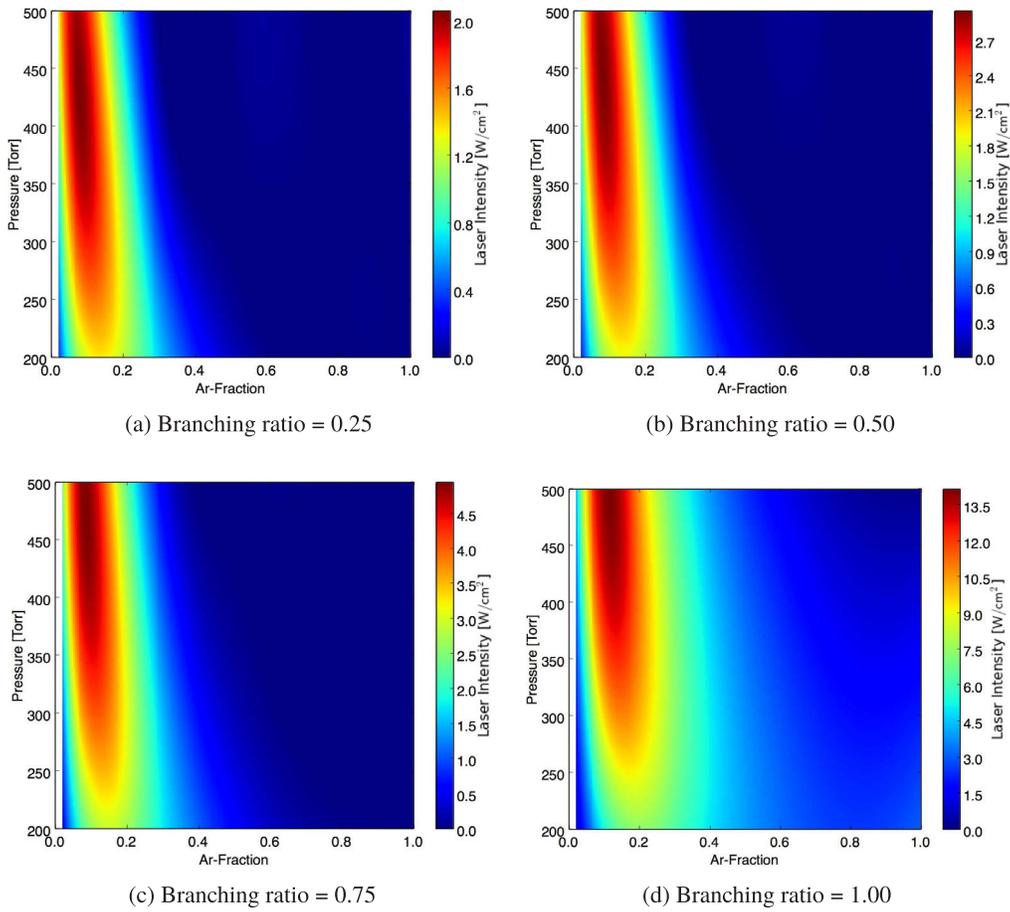

(d) Branching ratio = 1.00
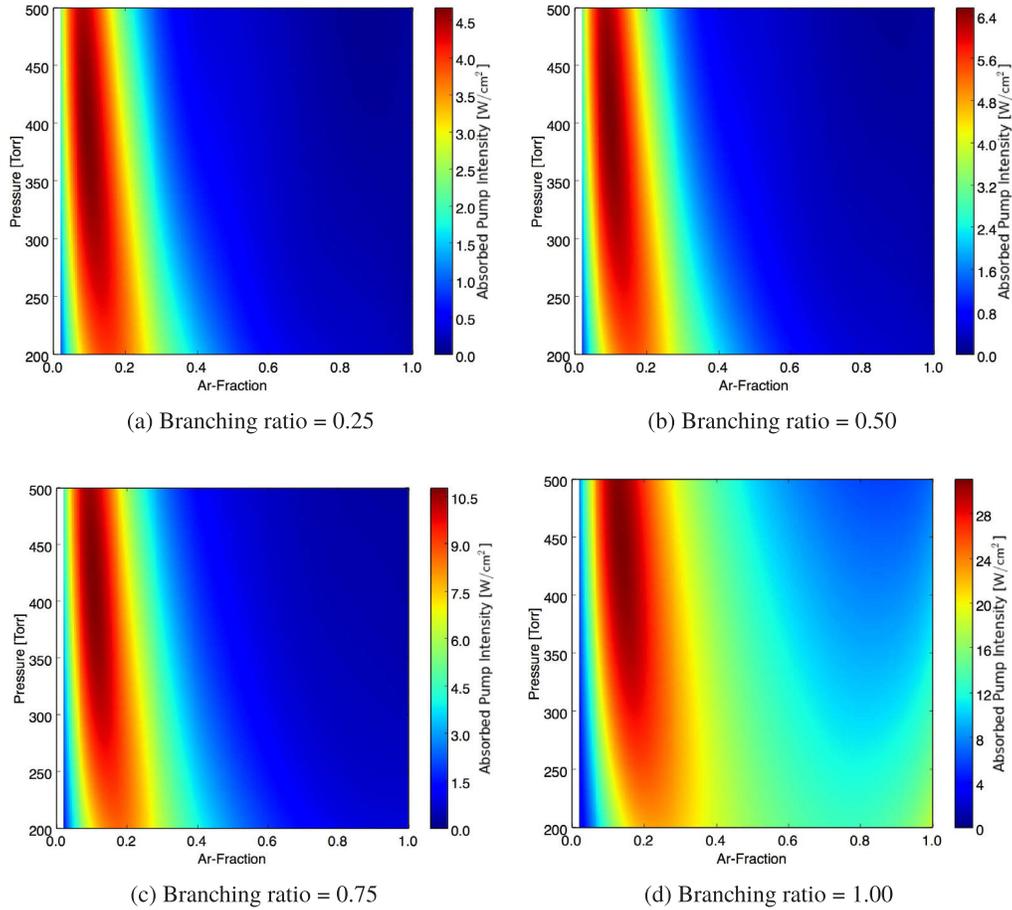
Fig. 3. Absorbed pump laser intensity as a function of Ar-fraction and pressure for variable branching ratios. Note the change in scale for the different images.

Analyzing the 460 Torr, 8% Ar-fraction scenario (corresponding to the peak laser intensity for a branching ratio of 0.50) as a function of branching ratio shows a nearly 7 fold increase in laser output and pump laser absorption as the branching ratio is increased from 0.02 to 1.00 (Fig. 5). To develop a simple kinetic description of the laser performance with respect to the branching ratio, we define the density ratios Ω, Γ, and Λ. The ratio of laser excited Ar species population collected in $Ar(1s_4)$ is defined as Ω:

$$\Omega \equiv \frac{[Ar(1s_4)]_l}{[Ar^*]_l}, \tag{7}$$

where $[Ar^*] = [Ar(1s_5) + Ar(1s_4) + Ar(2p_{10}) + Ar(2p_9) + Ar(2p_8)]$. As the branching ratio increases, Ω is reduced through a reduction in the $Ar(2p) + M \rightarrow Ar(1s_4) + M$ rates (Fig. 6). For a branching ratio of 0.02, nearly 90% of the Ar^* population is collected in $Ar(1s_4)$, which limits the population directly involved with laser kinetics. At a branching ratio of 1.00, approximately 50% of the Ar^* population is collected in $Ar(1s_4)$. Limiting the $Ar(1s_4)$ population enhances $Ar(1s_5)$, $Ar(2p_9)$, and $Ar(2p_{10})$ densities directly involved with laser performance, which increases the laser rates and output intensities.

The reduced electric field, E/N, is weakly affected by the inclusion of laser rates due to the minor role of stepwise ionization [8] and electron energy gained from superelastic collisions.

(a) Branching ratio = 0.25

(b) Branching ratio = 0.50

(c) Branching ratio = 0.75

(d) Branching ratio = 1.00

Fig. 4. Output laser intensity as a function of Ar-fraction and pressure for variable branching ratios. Note the change in scale for the different images.
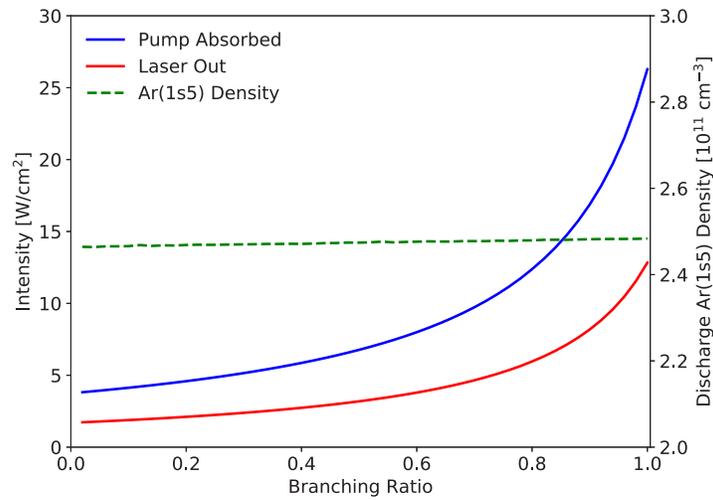
Fig. 5. Absorbed pump laser intensity, output laser intensity, and discharge metastable density as a function of branching ratio at a pressure of 460 Torr and 8% Ar-fraction.
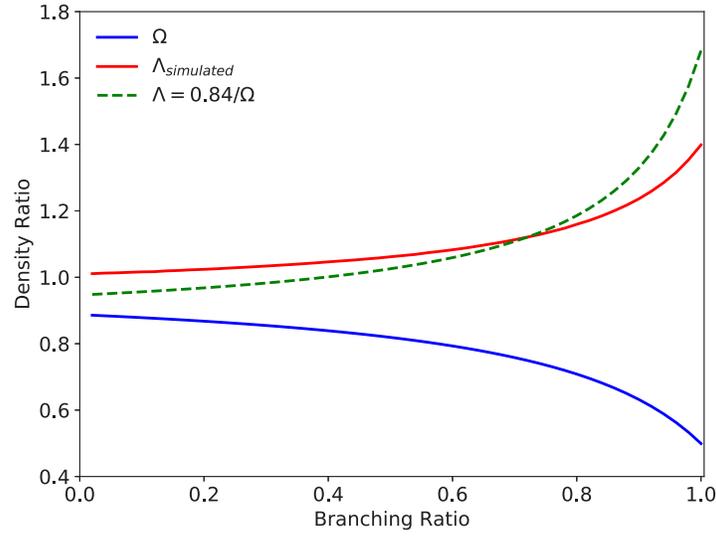
Fig. 6. Fraction of Ar^* population collected in $Ar(1s_4)$, Ω, and ratio of Ar^* density after laser initiation to discharge density, Λ, as a function of branching ratio at a pressure of 460 Torr and 8% Ar-fraction.

While the ratio of electron energy gained from superelastic collisions to the energy gained from the applied electric field increases as the diode laser elevates the $Ar(2p)$ densities, the ratio for the 460 Torr, 8% Ar-fraction scenario after diode pumping is on the order of 10^{-5} indicating a minor contribution to electron kinetics. As a result, the electron impact excitation rates of ground state Ar are weakly affected by the laser kinetics. Loss rates of Ar^* through excimer formation or radiation/quenching to the ground state are dependent on the $Ar(1s_4)$ and $Ar(1s_5)$ densities. A list of the primary loss reactions for Ar^* in a high pressure helium rich mixture is displayed in Table 2. With the assumption that the laser loss rates through $Ar(1s_5)$ are insignificant compared to loss rates through $Ar(1s_4)$ and that the excitation rates from the ground state are unchanged by laser kinetics, the discharge and laser loss rates are approximately equal:

$$
\begin{aligned}
&[Ar(1s_5)]_d \left(k_1 [He] + k_2 [Ar][Ar] + k_3 [Ar][He] \right) \\
&+ [Ar(1s_4)]_d \left(k_4 [Ar][Ar] + k_5 [Ar][He] + k_6 \right) \\
&\approx [Ar(1s_4)]_l \left(k_4 [Ar][Ar] + k_5 [Ar][He] + k_6 \right).
\end{aligned}
\tag{8}
$$

Before the inclusion of laser rates, roughly 90% of the Ar^* density is collected in $Ar(1s_5)$, with the other 10% in $Ar(1s_4)$. Solving for the ratio of laser $Ar(1s_4)$ density to total discharge Ar^* density provides the ratio defined as Γ:

$$
\begin{aligned}
\Gamma &\equiv \frac{[Ar(1s_4)]_l}{[Ar^*]_d} \\
&\approx \frac{0.9 \left(k_1 [He] + k_2 [Ar][Ar] + k_3 [Ar][He] \right) + 0.1 \left(k_4 [Ar][Ar] + k_5 [Ar][He] + k_6 \right)}{k_4 [Ar][Ar] + k_5 [Ar][He] + k_6}.
\end{aligned}
\tag{9}
$$

This simplified form of Γ allows for an understanding of the kinetics controlling the simulated change in Ar^* density. From the definition of Ω in Eq. 7, the following relationship is obtained:

$$
\Omega [Ar^*]_l = \Gamma [Ar^*]_d
\tag{10}
$$

$$
\implies \Lambda \equiv \frac{[Ar^*]_l}{[Ar^*]_d} = \frac{\Gamma}{\Omega},
\tag{11}
$$

where Λ is defined as the ratio of laser Ar^* density to the discharge Ar^* density.

Table 2. A list of primary loss reactions for the excited Ar species, Ar^*, in a high pressure helium rich mixture.

| Rate Coefficient Label	Reaction	Rate Coefficient [1/s, cm^3/s, or cm^6/s]	Ref.
k_1	$Ar(1s_5) + He \rightarrow Ar + He$	1.60×10^{-14}	[20][a]
k_2	$Ar(1s_5) + Ar + Ar \rightarrow Ar_2^* + Ar$	$3.60 \times 10^{-31} T_{gas}^{-0.6}$	[21]
k_3	$Ar(1s_5) + Ar + He \rightarrow Ar_2^* + He$	$1.80 \times 10^{-31} T_{gas}^{-0.6}$	[21][b]
k_4	$Ar(1s_4) + Ar + Ar \rightarrow Ar_2^* + Ar$	0.95×10^{-32}	[21]
k_5	$Ar(1s_4) + Ar + He \rightarrow Ar_2^* + He$	0.48×10^{-32}	[21][b]
k_6	$Ar(1s_4) \rightarrow Ar + \hbar\omega$	$1.20 \times 10^8 / 700$	[22][c]

[a]Reaction may be a proxy for quenching due to impurities [23]
[b]Assuming three-body rate coefficients with He as the third body are 1/2 the rate coefficient for Ar as the third body [3]
[c] Reduction by a factor of 700 due to radiation trapping [24,25]

At a pressure of 460 Torr and a mixture of 8% Ar in He, Γ from Eq. 9 is estimated to be 0.84. This estimate along with the simulated values of Ω and Λ directly from the zero-dimensional model are displayed in Fig. 6. The two approaches provide a similar trend for Λ as a function of branching ratio. To reach a steady-state after laser ignition, an overall increase in Ar^* density is required to increase the laser loss rates through $Ar(1s_4)$ so that they are equal to the discharge loss rates. For a constant pressure and Ar-fraction Λ shows an increase from 1.0 to 1.4 as the branching ratio is increased from 0.02 to 1.00.

The Ar^* loss rates are functions of pressure and Ar-fraction. Repeating the calculations for a pressure of 350 Torr and a mixture of 10% Ar in He provides the ratios displayed in Fig. 7. At this pressure and Ar-fraction, Γ calculated from Eq. 9 provides a value of 0.68. Unlike the 460 Torr scenario, which predicts an increase in Ar^* densities due to laser kinetics, the 350 Torr scenario shows a reduction in Ar^* densities caused by laser ignition for branching ratios below approximately 0.80. At this lower pressure, the reduced discharge loss rates allows for a
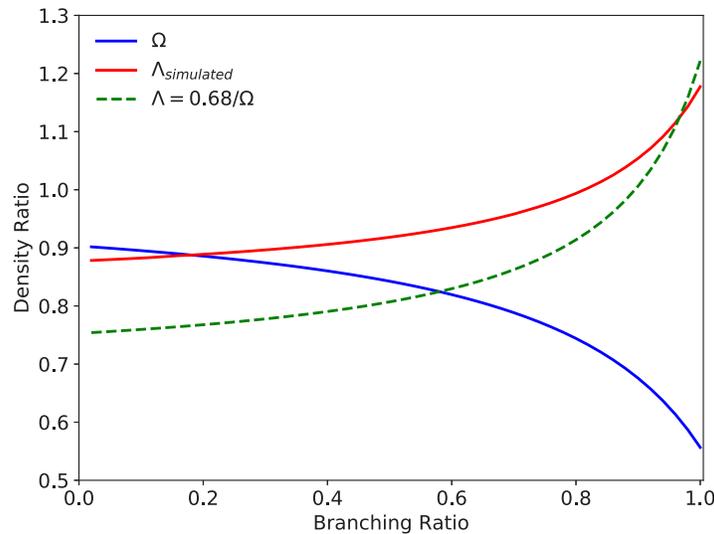
Fig. 7. Fraction of Ar^* population collected in $Ar(1s_4)$, Ω, and ratio of Ar^* density after laser initiation to discharge density, Λ, as a function of branching ratio at a pressure of 350 Torr and 10% Ar-fraction.

reduced laser $Ar(1s_4)$ density to match the discharge loss rates, which causes a reduction in the Ar^* densities after laser ignition.

The optical to optical conversion efficiency, defined as the ratio of the output laser intensity to the absorbed diode pump laser intensity, is weakly related to the branching ratio. For the 8% Ar-fraction at 460 Torr, a change of less than 4% is observed over the range of branching ratios, increasing from 45% to 49% as the branching ratio increases from 0.02 to 1.00. Similar behavior is observed in the optical to optical conversion efficiency associated with the peak output laser intensities as a function of branching ratio (Table 1). Overall, the range of efficiencies is moderately less than the experimentally measured efficiency of 55% [2].

4. Conclusions

Simulations of an optically pumped rare gas laser are performed as a function of the $Ar(2p) + M \rightarrow Ar(1s) + M$ branching ratio using a radio frequency dielectric barrier discharge as the source of metastable production. A time dependent zero-dimensional discharge model including laser kinetics is used to calculate pump laser absorption and output laser intensities over a range of Ar-He mixtures from 200-500 Torr. While the discharge metastable densities show a decrease with increasing pressure, the peak output laser intensities occur at higher pressures due to the increased $Ar(2p_9) + M \rightarrow Ar(2p_{10}) + M$ relaxation rates and broadened pump laser absorption linewidths. Additionally, as a result of the decrease in the detrimental $Ar(2p) + M \rightarrow Ar(1s_4) + M$ rates, the peak output intensity shifts to higher pressures as the branching ratio is increased. A large increase in pump laser absorption and output laser intensity are observed as the branching ratio to $Ar(1s_5)$ is increased, resulting in a factor of 7 increase in the peak output intensity as the branching ratio is increased from 0.25 to 1.00.

The $Ar(1s_4)$ species plays a key role in laser kinetics. As the branching ratio increases, the fraction of Ar^* populations collected in $Ar(1s_4)$ decreases, which increases the densities of the species directly involved with laser performance: $Ar(1s_5)$, $Ar(2p_9)$, and $Ar(2p_{10})$. Additionally, the electron excitation rates of ground state Ar are weakly affected by the introduction of the laser kinetics. As a result of the nearly constant electron excitation rates and the redistribution of Ar^* densities, the total laser Ar^* density evolves to match the discharge loss rates. The laser ignition can cause an increase or decrease in the Ar^* density, depending on the Ar-fraction, pressure, and branching ratio.

While the $Ar(2p) + M \rightarrow Ar(1s) + M$ branching ratios are not well known, their effect on laser kinetics and intensities is significant. To provide a more complete analysis of the branching ratio impact, the $Ar(1s_3)$ and $Ar(1s_2)$ levels should be included in the laser kinetics model. Additionally, kinetic measurements of the branching ratio would be beneficial to understanding the limitations to optically pumped rare gas laser performance.

Disclosures

The authors declare no conflicts of interest.

References

1. J. Han, L. Glebov, G. Venus, and M. C. Heaven, "Demonstration of a diode-pumped metastable Ar laser," Opt. Lett. **38**(24), 5458–5461 (2013).

2. W. Rawlins, K. Galbally-Kinney, S. Davis, A. Hoskinson, J. Hopwood, and M. Heaven, "Optically pumped microplasma rare gas laser," Opt. Express **23**(4), 4804–4813 (2015).

3. A. Demyanov, I. Kochetov, and P. Mikheyev, "Kinetic study of a CW optically pumped laser with metastable rare gas atoms produced in an electric discharge," J. Phys. D: Appl. Phys. **46**(37), 375202 (2013).

4. Z. Yang, G. Yu, H. Wang, Q. Lu, and X. Xu, "Modeling of diode pumped metastable rare gas lasers," Opt. Express **23**(11), 13823–13832 (2015).

5. J. Han, M. C. Heaven, G. D. Hager, G. B. Venus, and L. B. Glebov, "Kinetics of an optically pumped metastable Ar laser," in *SPIE LASE* (International Society for Optics and Photonics, 2014), p. 896202.

6. R. Chang and D. Setser, "Radiative lifetimes and two-body deactivation rate constants for Ar(3p5, 4p) and Ar(3p5, 4p) states," J. Chem. Phys. **69**(9), 3885–3897 (1978).

7. J. Han and M. C. Heaven, "Kinetics of optically pumped Ar metastables," Opt. Lett. **39**(22), 6541–6544 (2014).

8. D. J. Emmons, "Analysis of Ar(1s5) metastable populations in high pressure argon-helium gas discharges," Ph.D. thesis (Department of Physics, Air Force Institute of Technology, 2017).

9. D. J. Emmons, D. E. Weeks, B. Eshel, and G. P. Perram, "Metastable Ar(1s5) density dependence on pressure and argon-helium mixture in a high pressure radio frequency dielectric barrier discharge," J. Appl. Phys. **123**(4), 043304 (2018).

10. J. Han, M. Heaven, P. Moran, G. Pitz, E. Guild, C. Sanderson, and B. Hokr, "Demonstration of a CW diode-pumped Ar metastable laser operating at 4 W," Opt. Lett. **42**(22), 4627–4630 (2017).

11. J. Han, C. Sanderson, B. Hokr, C. Ballmann, A. Clark, and M. Heaven, "Optically pumped rare gas lasers," *XXII International Symposium on High Power Laser Systems and Applications*, vol. 11042 (International Society for Optics and Photonics, 2019), p. 1104202.

12. P. A. Mikheyev, J. Han, A. Clark, C. Sanderson, and M. C. Heaven, "Production of Ar and Xe metastables in rare gas mixtures in a dielectric barrier discharge," J. Phys. D: Appl. Phys. **50**(48), 485203 (2017).

13. S. Pancheshnyi, B. Eismann, G. Hagelaar, and L. Pitchford, *Computer code ZDPlasKin, University of Toulouse, LAPLACE*, CNRS–UPS–INP, Toulouse, France, http://www.zdplaskin.laplace.univ-tlse.fr (2008).

14. G. Hagelaar and L. Pitchford, "Solving the Boltzmann equation to obtain electron transport coefficients and rate coefficients for fluid models," Plasma Sources Sci. Technol. **14**(4), 722–733 (2005).

15. D. J. Emmons and D. E. Weeks, "Kinetics of high pressure argon-helium pulsed gas discharge," J. Appl. Phys. **121**(20), 203301 (2017).

16. B. Eshel, C. A. Rice, and G. P. Perram, "Pressure broadening and shift rates for Ar(s–p) transitions observed in an Ar–He discharge," J. Quant. Spectrosc. Radiat. Transfer **179**, 40–50 (2016).

17. N. D. Zameroski, G. D. Hager, W. Rudolph, and D. A. Hostutler, "Experimental and numerical modeling studies of a pulsed rubidium optically pumped alkali metal vapor laser," J. Opt. Soc. Am. B **28**(5), 1088–1099 (2011).

18. G. D. Hager and G. Perram, "A three-level analytic model for alkali metal vapor lasers: part I. Narrowband optical pumping," Appl. Phys. B: Lasers Opt. **101**(1-2), 45–56 (2010).

19. R. J. Beach, W. F. Krupke, V. K. Kanz, S. A. Payne, M. A. Dubinskii, and L. D. Merkle, "End-pumped continuous-wave alkali vapor lasers: experiment, model, and power scaling," J. Opt. Soc. Am. B **21**(12), 2151–2163 (2004).

20. J. Han and M. Heaven, Personal Communication (2016).

21. W. Wieme and J. Lenaerts, "Excimer formation in argon, krypton, and xenon discharge afterglows between 200 and 400 K," J. Chem. Phys. **74**(1), 483–493 (1981).

22. A. Kramida, Y. Ralchenko, and J. Reader, and NIST ASD Team, *NIST atomic spectra database (Ver. 5.3)*, http://physics.nist.gov/asd (2015).

23. I. Stefanović, T. Kuschel, S. Schröter, and M. Böke, "Argon metastable dynamics and lifetimes in a direct current microdischarge," J. Appl. Phys. **116**(11), 113302 (2014).

24. T. Holstein, "Imprisonment of resonance radiation in gases," Phys. Rev. **72**(12), 1212–1233 (1947).

25. S. G. Belostotskiy, T. Ouk, V. M. Donnelly, D. J. Economou, and N. Sadeghi, "Time-and space-resolved measurements of Ar(1s5) metastable density in a microplasma using diode laser absorption spectroscopy," J. Phys. D: Appl. Phys. **44**(14), 145202 (2011).